Renewable Energy 101 (2017) 1379–1389

Contents lists available at ScienceDirect

Renewable Energy

journal homepage: www.elsevier.com/locate/renene

Design, simulation and experimental characterization of a novel parabolic trough hybrid solar photovoltaic/thermal (PV/T) collector

Bennett K. Widyolar [a], Mahmoud Abdelhamid [a, *], Lun Jiang [a], Roland Winston [a], Eli Yablonovitch [b], Gregg Scranton [b], David Cygan [c], Hamid Abbasi [c], Aleksandr Kozlov [c]

[a] University of California - Merced, 5200 Lake Rd, Merced, CA 95343, USA
[b] University of California - Berkeley, Berkeley, CA, USA
[c] Gas Technology Institute, Des Plaines, IL, USA

ARTICLE INFO

Article history:
Received 26 May 2016
Received in revised form
17 August 2016
Accepted 6 October 2016
Available online 8 October 2016

Keywords:
Hybrid concentrated photovoltaic thermal (PV/T) system
Gallium arsenide (GaAs) solar cells
Compound parabolic concentrator (CPC)
Solar thermal collector
Parabolic trough

ABSTRACT

A novel hybrid solar concentrated photovoltaic thermal (PV/T) collector is designed, simulated, and tested. The PV/T system uses a parabolic trough to focus sunlight towards a nonimaging compound parabolic concentrator (CPC) that is formed of single junction Gallium Arsenide (GaAs) solar cells to simultaneously generate electricity and high temperature thermal power. The GaAs cells generate electricity from high energy photons and reflect low energy photons towards the high temperature absorber, thus maximizing the exergy output of the system. The two-stage design also allows the thermal absorber to reach a geometric concentration ratio of ~60×, which is significantly higher than other PV/T systems and enables the absorber to reach high temperatures even under partial utilization of the solar spectrum. The modelled exergy efficiency with a thermal absorber operating at 500 °C is 37%. In the experimental setup, the maximum outlet temperature reached was 365 °C with a thermal efficiency of around 37%. The direct solar to electric efficiency from the GaAs cells was 8%. This design is capable of producing electricity directly along with high temperature thermal energy that can be stored for dispatchable electricity production and has the potential to significantly improve the exergy efficiency of parabolic troughs plants.

1. Introduction

High utilization of solar energy, renewable, clean, and abundant source, is an important component for future energy needs that will ensure energy independence and low environmental impact [1]. Solar energy is available at no cost, but efficient collection, storage, and use of this energy in an economical way remains a challenge. Hybrid photovoltaic/thermal (PV/T) systems increase system efficiency by using a combination of PV devices and solar thermal collectors to produce both heat and electricity. Incident photon energy on a PV device that does not produce electricity builds up as heat. Instead of wasting this energy, hybrid systems collect it using a heat transfer fluid (HTF). The concept of PV/T was developed in the 1970s [2] and since then a significant amount of research and development work on PV/T technology has been done as extensively reviewed in Refs. [3–13]. PV/T systems differ in fluid temperature, HTF type, concentration ratio, PV cell type, thermal efficiency, and electrical efficiency. The most common HTFs used in PV/T technologies are air [3,10,14] or water [12,15,16]. While air systems are generally simpler, water based PV/T systems are more efficient due to the higher heat capacity of water. Both of these designs are limited to relatively low temperatures applications. The performance of a PV/T system depends on the PV device as well, with most systems using mono-crystalline (Mono-Si), multi-crystalline (Multi-Si), or thin film amorphous silicon (a-Si) [17,18]. Crystalline silicon solar cell types are more efficient, but are affected much more negatively at higher working temperatures compared to the thin film PVs [19–21]. Most studies of PV/T collectors deal with flat plate collectors [7,12], or low concentration nonimaging systems [22,23]. In Ref. [22] the authors reported on a water-cooled PV/T system with a 4× concentration ratio using compound parabolic concentrators (CPC) with a maximum fluid temperature of 65 °C. In Ref. [23], the concentrator was designed using a Fresnel lens and flat mirrors to get a uniformly concentrated irradiation on the solar cells. To date there has been little to no work in the field of medium to high concentration PV/T collectors

* Corresponding author.
E-mail address: mabdelhamid@ucmerced.edu (M. Abdelhamid).

http://dx.doi.org/10.1016/j.renene.2016.10.014
0960-1481/

Nomenclature

C	final concentration ratio of the system
C_{1st}	primary concentrator ratio
C_{2nd}	secondary concentrator ratio
Φ	half rim angle [°]
θ	acceptance Angle [°]
A_1	primary concentrator aperture area [m^2]
A_2	secondary concentrator aperture area [m^2]
A_3	absorber area [m^2]
r	radius [m], Which is focal length
G_{abs}	amount of radiation absorbed by the high temperature absorber
G_{cell_inc}	the amount of radiation incident upon the GaAs cells
T_{in}	inlet temperature of fluid stream [°C]
T_{out}	outlet temperature of fluid stream [°C]
T_{cold}	environmental temperature (=310 K)
T_{hot}	hot stream temperature [K]
T_s	absorber outer surface node [°C]
T_f	fluid node temperature [°C]
$T_{f,out}$	outlet temperature [°C]
h	heat transfer coefficient [W/m^2-K]
dx	node length [m]
k	thermal conductivity [W/m K]
ε	emissivity
G_{cell_abs}	the amount of radiation absorbed by the GaAs cells
$\dot{m}$	mass flow rate of fluid [kg/s]
c_p	heat capacity of fluid [kJ/kg-K]
$Q_{High\ temperature\ stream}$	thermal power generated by high temperature stream [kW]
η_{GaAs}	efficiency of GaAs cells at operating temperature
T_{cell}	cell temperature [°C]
$Q_{low\ temperature\ stream}$	thermal power generated by low temperature stream [kW]
Q_{GaAs}	electrical power generated by GaAs cells [kW]
Q_{bulk_loss}	bulk thermal loss from low temperature fluid stream [kW]
G	incoming system irradiance [kW]
$\eta_{exergy,\ system}$	total system exergy efficiency
$\eta_{energy,\ high\ temp}$	energy efficiency of the high temperature stream
$\eta_{energy,\ low\ temp}$	energy efficiency of the low temperature stream
$\eta_{electrical}$	electrical efficiency
η_{energy}	energy efficiency from the high and low temperature streams
T_i	absorber inner surface node [°C]
$T_{f,in}$	inlet fluid temperature [°C]
Q	thermal Power [kW]
A	surface area [m^2]
D_0	outer diameter [m]
D_i	inner diameter [m]
σ	stefan-Boltzmann constant [W m^{-2} K^{-4}]

operating at high temperature due to increased system complexity added by cooling mechanisms, trackers, and solar cell performance at elevated temperatures. The combined heat and power solar system (CHAPS) [17] consists of glass-on-metal mirrors that focus light onto Mono-Si solar cells with a geometric concentration ratio of 37×. It is water cooled and reaches an outlet temperature of 80 °C. The use of high efficiency thin films solar cells such as Gallium Arsenide (GaAs) in PV/T systems is rarely investigated in the literature, despite the fact that GaAs cells have better efficiencies and temperature coefficients than silicon solar cells [24].

The purpose of this study is to design, simulate, and test a novel parabolic trough hybrid PV/T solar collector capable of producing electricity directly and high temperature thermal energy to be stored for on-demand electricity production. Using nonimaging optics the receiver is transformed into a spectrum-splitting device. The proposed system uses world record single-junction GaAs solar cells, which have a very sharp band gap cutoff, allowing them to produce electricity from high energy photons while reflecting lower energy photons to a thermal absorber. This unique double stage concentrator design achieves a concentration ratio ~60×, which is significantly higher than conventional PV/T systems. This helps achieve high temperatures under partial utilization of the solar spectrum and maximizes the exergy efficiency output of the system.

2. Design of two-stage concentrator of hybrid PV/T system

The proposed optical system uses a two-stage concentrator as shown in Fig. 1. Optimization of the primary and secondary concentrators is based on the half rim angle (ϕ) of the system (Eqs. (1)–(5)) [25]. The closer ϕ is to 0°, the closer the concentration ratio is to theoretical maximum. A 0° ϕ, however, results in an infinitely long focus length with a flat surface as the primary reflector. The secondary concentrator in this case will also be infinitely long. Due to practical considerations we chose $\phi = 45°$, which reaches about 70% of the ideal concentration.

$$C_{1st} = \frac{A_1}{A_2} \tag{1}$$

$$C_{2nd} = \frac{A_2}{A_3} \tag{2}$$

$$C_{1st} \le \frac{2rsin\varphi}{\frac{2r\theta}{cos\varphi}} = (sin\varphi cos\varphi)/\theta \tag{3}$$

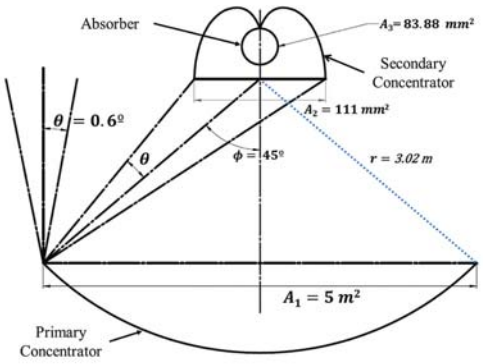

Fig. 1. Double stage concentrator of the proposed optic design.

$$C_{2nd} \leq 1/\sin(\varphi) \tag{4}$$

$$C = C_{1st}, C_{2nd} = \cos(\varphi)/\theta \tag{5}$$

where, C: final concentration ratio of the system, C_{1st}: primary concentrator ratio, C_{2nd}: secondary concentrator ratio, θ: acceptance Angle [°], A_1: primary concentrator aperture area [m^2], A_2: secondary concentrator aperture area [m^2], A_3: absorber area [m^2], and r: radius [m].

For this design, θ was chosen to be 0.6° to accommodate the sun disk angle (0.27°) with a margin for error introduced by optical and mechanical inaccuracies.

The main components of the proposed system are shown in Fig. 2. The hybrid PV/T receiver includes a nonimaging compound parabolic concentrator (CPC) which provides secondary concentration to the high temperature thermal absorber. The receiver is made of several sub-components including (a) aluminum minichannel struts, which roughly approximate the "wings" of the CPC and serve as fluid channels to provide active cooling of the cells, (b) thin film GaAs cells which are applied directly to the aluminum minichannels, (c) curved mirrors to form the involute portion of the CPC where flat minichannels cannot, (d) selectively coated absorber which receives concentrated light from the CPC and serves as the high temperature fluid channel, (e) outer glass tube which allows the entire receiver to be evacuated for heat loss reduction.

The parabolic mirror (primary concentrator) reflects and focuses incoming direct beam solar irradiance toward the hybrid PV/T receiver and as this light passes through the glass tube enclosure it strikes either (a) the GaAs covered minichannels, (b) the curved involute mirror portion of the CPC, or (c) the high temperature absorber directly. Light that strikes the GaAs cells is spectrally split based on the 870 nm bandgap cutoff, with about 90% of photons with energy higher than the bandgap being absorbed and converted to electricity or heat, and about 92% of photons with energy lower than the bandgap being reflected towards the high temperature absorber. Thus the system produces electricity directly from the PV cells and low grade heat by actively cooling the cells via the minichannel substrate. The high temperature absorber receives the spectrally split light reflected from the GaAs cells as well as light reflected from the curved mirror involute portion of the CPC and light that strikes the absorber from the primary parabolic mirror directly.

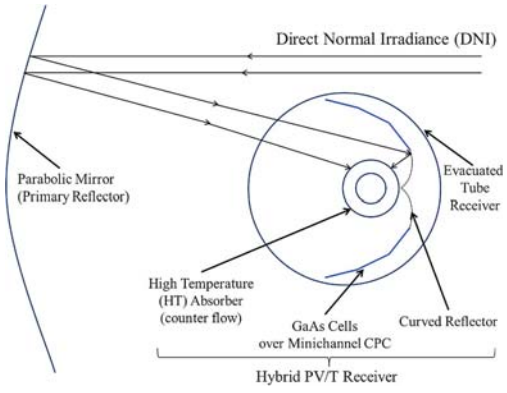

Fig. 2. Two-stage concentrator of hybrid PV/T system schematic.

The primary parabolic mirror and support structures are shown in Fig. 3 (a). The primary parabolic mirror (A_1) is 5 m^2 and made of ReflecTech [26]. The receiver is located at the focus (distance $r = 3.02$ m from the mirror surface, See Fig. 1). Standard parabolic mirrors generally use a half rim angle (ϕ) of 90° to maximize illumination of the absorber surface. Since we are using a secondary concentrator which evenly illuminates the entire absorber surface area (A_3), however, we employ $\phi = 45°$ so that the secondary concentrator is still able to provide additional concentration.

The design of the hybrid PV/T receiver, as illustrated in Figs. 3e and 4, is based on nonimaging optics and previous work on inserted internal CPC reflectors [27]. Standard parabolic troughs generally use a 70 mm diameter absorber [28], however, the angular potential of the surface is not fully utilized. This problem is solved by using a secondary concentrator that illuminates the entire surface of the absorber.

A system acceptance angle of 0.6° creates a light beam 100 mm width at the focus of the parabolic mirror. With a 10% safety factor, we designed the CPC to have an aperture width of around 110 mm. To fit within the 120 mm inner diameter glass tube, the CPC was truncated to 94% of the original aperture width and 66% of the original height. Truncation as well as the approximation of the CPC shape with flat minichannels resulted in a reduced optical efficiency of 91% compared to an ideal CPC.

The final system concentration (C) is calculated based on the design specifications (Eqs. (6)–(8)). C_{1st} is the ratio between the primary parabolic mirror and the CPC aperture, C_{2nd} is the ratio between the aperture of the CPC to the absorber surface. A_1 is the aperture area of the parabolic mirror, A_2 is CPC aperture area, and A_3 is the absorber area.

$$C_{1st} = \frac{A_1}{A_2} = \frac{5000\ mm}{111.12\ mm} = 45X \tag{6}$$

$$C_{2nd} = \frac{A_2}{A_3} = \frac{111.12\ mm}{\pi * 26.7\ mm} = 1.324X \tag{7}$$

$$C = C_{1st} \cdot C_{2nd} = 59.6X \tag{8}$$

As explained, the proposed design achieves a geometric concentration ratio of approximately 60× on the thermal absorber which allows it to operate at similar or higher temperatures compared to conventional parabolic trough systems even under partial utilization of the solar spectrum. The high temperature absorber (see Fig. 3d) was constructed of 3/4″ Schedule 5 stainless steel with an outer diameter of 26.7 mm. It was selectively coated by Himin Solar Co. and has a solar weighted absorption greater than 95% and an emissivity of 0.08 at 300 °C [29].

The emissivity of the coating at different temperatures was estimated by comparing blackbody emission at with the spectral emissivity data provided by Himin Solar Co. As an example, the red line in Fig. 5 depicts the spectral emissivity of the coating while the blue line represents the emission curve of a blackbody at 500 °C. Multiplication of the two produces a spectral emission curve for the coating at 500 °C, represented by the green line. The area under the green curve divided by the total area under the blue curve gives an estimate of the emissivity at this new temperature. The total emissivity of this coating at 500 °C is estimated to be 0.14.

The solar cells used are state-of-the-art single junction GaAs cells manufactured by Alta Devices (see Fig. 3b). Because of their sharp bandgap cutoff at 870 nm with 90% absorption at sub-bandgap wavelengths and 92% reflectance at wavelengths above the bandgap as shown in Fig. 6, they are also very efficient spectrally selective reflectors. The solar to electric efficiency of these cells is 28.8% at room temperature with a temperature coefficient of

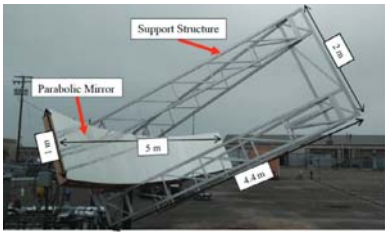

(a)Primary reflector (parabolic mirror) and support structure

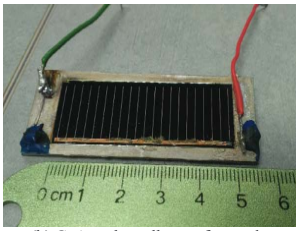

(b) GaAs solar cell manufactured by Alta Devices

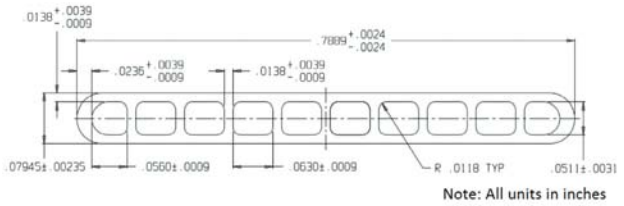

(c) Minichannel design

(d) High temperature (HT) absorber

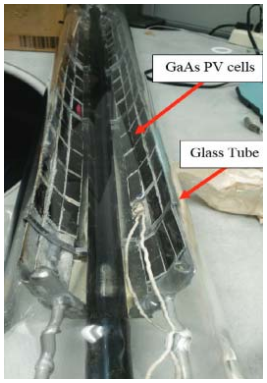

(e) Hybrid PV/T receiver

Fig. 3. System components.

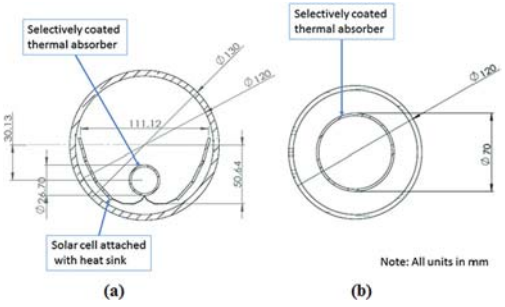

Fig. 4. (a) Hybrid PV/T receiver (b) Standard receiver.

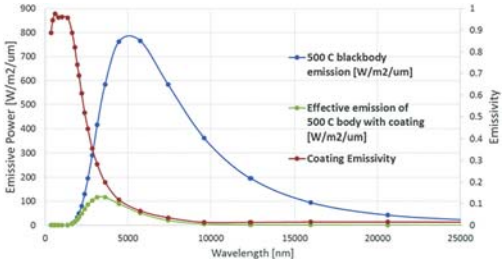

Fig. 5. Emissivity of Himin Solar Co. coating at 500 °C.

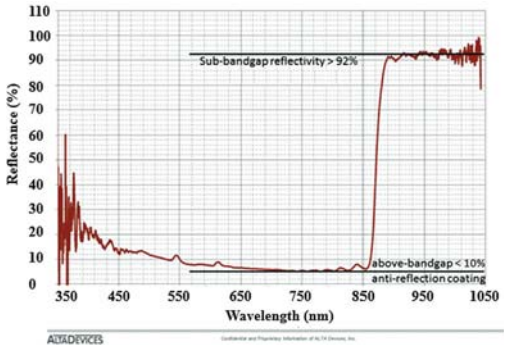

Fig. 6. Spectral reflectance of Alta Devices' GaAs cell.
Source: Alta Devices Co.

−0.08%/°C [30]. In the proposed design the GaAs cells occupy only 2.4% of A_1, allowing the system to be more affordable, while still receiving 41.6% of the incoming direct beam irradiance incident on the trough.

The wings of the CPC are approximated by three 20 mm (~0.79 inch) long segments of minichannels (see Fig. 3c). The involute portion of the CPC is formed from Alanod Miro-Sun which has a total solar reflectance of approximately 89% [31]. The GaAs cells were glued to the minichannels with a thermally conducting and electrically isolating thermal paste (Omega-Therm). Photons that are absorbed but do not generate electricity become heat, which is removed by conduction through the thermal past and mini-channels and convection into the cooling fluid stream. Overall the cells serve three purposes: (1) spectral splitter/concentrators, (2) selective low temperature thermal absorbers, and (3) electricity generators.

3. Performance models

3.1. Optical performance model

An optical model of the system was developed and analysis was performed using LightTools illumination design software [32]. The optical model includes spectral surface properties of all components. Reflectance of the GaAs cell in the infrared region was assumed constant by extrapolation of the reflectance of the longest wavelength measured, and assumed constant in the UV region by extrapolation of the lowest reflectivity measured (see Fig. 7). The

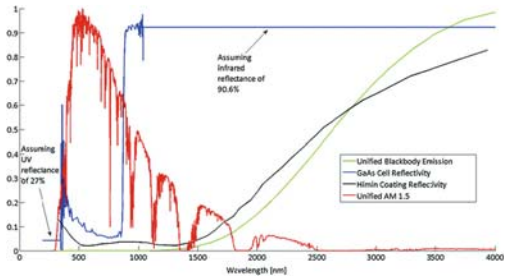

Fig. 7. GaAs cell and Himin coating reflectivity versus blackbody emission and AM 1.5.

Table 1
Optical simulation results.

	Percent of incoming light
Light incident on solar cells	42%
Light incident on involute mirror	15%
Light incident on absorber	50%
Light absorbed by cells (electricity + heat)	26%
Light absorbed by involute mirror	1%
Light absorbed by absorber	47%

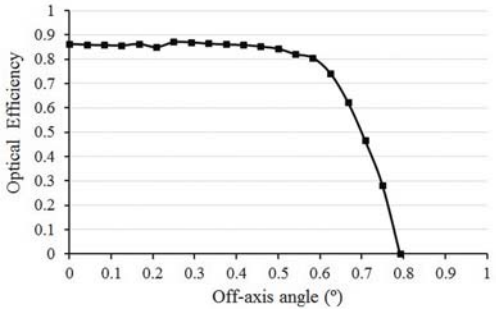

Fig. 8. System optical performance for off-axis angles.

AM 1.5 and 500 °C blackbody emission curves presented in Fig. 7 are unified, meaning values at all wavelengths are divided by the maximum value to adjust the data to be between 0 and 1.

Optical modelling of the complete system was performed using uniformly distributed rays within a 0.8° cone. The uniform angular spread within a 0.8° cone was chosen to simulate the effects of sun disk angle, tracking error, and optical misalignment of the system [33]. Of the total incoming irradiance to the system, 82% of the light is incident on the aperture of the 2nd concentrator (losses from

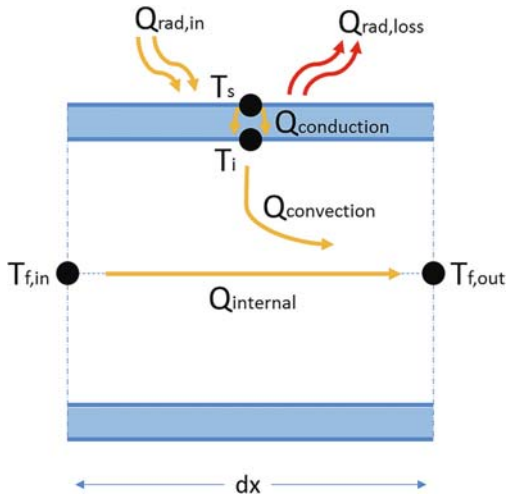

Fig. 9. Finite element analysis of absorber tube.

Table 2
Thermal model calculations.

Parameter	Diagram	Equations used for analysis
Absorber outer surface node (T_s)	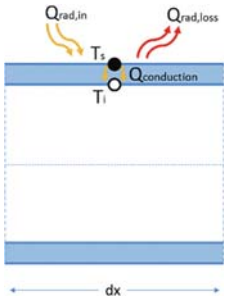	$Q_{in} = Q_{out}$ (9) $Q_{rad,In} = Q_{rad,loss} + Q_{conduction}$ (10) $Q_{rad,In} = \frac{G_{abs}}{n}$ (11) $G, \eta_{o,abs} = A_s \varepsilon \sigma T_s^4 + \frac{2\pi k dx}{\ln \frac{D_o}{D_i}}(T_s - T_i)$ (12) $G = \mathrm{DNI}, A_{aperture}$ (13)
Absorber inner surface node (T_i)	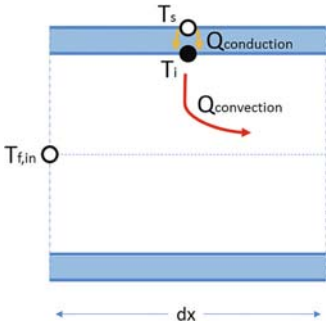	$Q_{conduction} = Q_{convection}$ (14) $\frac{2\pi k dx}{\ln \frac{D_o}{D_i}}(T_s - T_i) = hA_i\left(T_i - T_{f,in}\right)$ (15)
Fluid node (T_f)	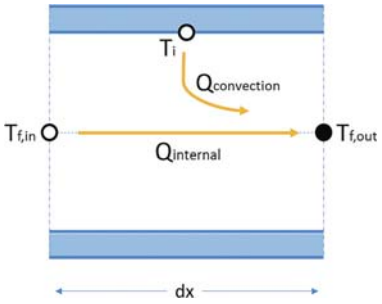	$Q_{convection} = Q_{heat.capacity}$ (16) $hA_i\left(T_i - T_{f,in}\right) = \dot{m} c_p \left(T_{f,out} - T_{f,in}\right)$ (17)

Q is heat; h is heat transfer coefficients; A is surface area; dx node length; c_p is heat capacity; m is mass flow rate; k thermal conductivity; D_0 is outer diameter; D_i is inner diameter; ε emissivity; σ Stefan-Boltzmann constant; $A_{aperture}$ is aperture area of parabolic trough; n is number of nodes.

Table 3
Thermal performance model parameters.

Thermal Model Parameters	Value
Emissivity of selective coating at 300 °C	0.08
Emissivity of selective coating at 500 °C	0.14
GaAs cell efficiency (η_{GaAs}) at 200 °C	14.8%
Emissivity of GaAs cell	0.10
Emissivity of aluminum minichannels	0.08
Thermal conductivity of stainless steel	20 W/m-K
Absorptivity of glass in infrared region	100%

reflection and glass transmittance). Of the incoming DNI, 47% is captured at the absorber and 26% is captured by the solar cells and converted into electricity or low grade heat (see Table 1).

Optical performance of the system for off-axis angles was simulated and the results are presented in Fig. 8. Beyond 0.6°, the optical efficiency drops significantly.

The optical model generates three key performance parameters which are used to calculate the thermal performance of the system: radiation absorbed by the absorber (G_{abs}), radiation incident on the GaAs cells (G_{cell_inc}), and the amount of radiation absorbed by the GaAs cells (G_{cell_abs}).

3.2. Thermal performance model

Heat transfer through the high temperature counter-flow absorber tube is determined using a finite element analysis (FEA) model constructed in MatLab [34] using the absorbed radiation input from the optical model. Fig. 9 shows the radiation balance between the hot absorber surface and the inside of the absorber tube for single node length (dx), while Table 2 summarizes the FEA calculations in each node of absorber outer surface node (T_s), absorber inner surface node (T_i), and fluid node (T_f), inlet fluid temperature ($T_{f,in}$) and outlet temperature ($T_{f,out}$). The simulation is performed for a meter-long absorber containing 50 nodes. For simplicity, it was assumed the GaAs cells would not absorb any of the emitted radiation from the absorber because they are highly reflective in the infrared region. Table 3 shows the thermal performance model parameters used.

The model determines the outlet temperature of the high temperature fluid stream based on a set input temperature, flow rate, and direct beam solar irradiance to the system and the thermal output ($Q_{high\ temperature\ stream}$) is calculated using Eq. (18).

$$Q_{high\ temperature\ stream} = \dot{m} c_p (T_{out} - T_{in}) \tag{18}$$

Where;

$\dot{m}$: Mass flow rate of fluid [kg/s]

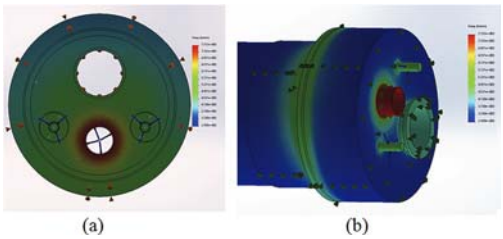

Fig. 10. (a) Radiative heat loss from interior stainless steel end cap, (b) Heat loss through 50.8 mm (2″) Fiberglass Insulation.

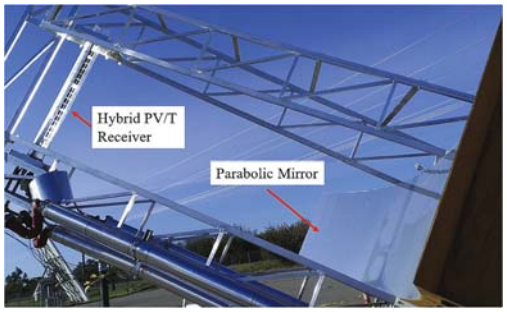

Fig. 11. Parabolic mirror and hybrid PV/T receiver.

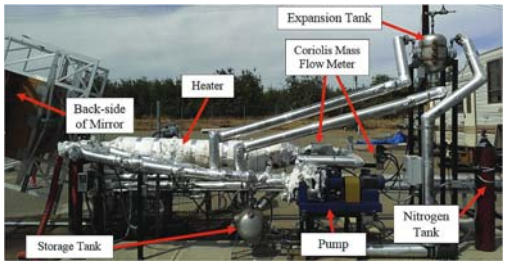

Fig. 12. High temperature loop setup.

c_p: Heat capacity of fluid [kJ/kg-K]
T_{out}: Outlet temperature of fluid stream [°C]
T_{in}: Inlet temperature of fluid stream [°C]

The temperature coefficient of the GaAs cells is well documented [30] and their solar to electric efficiency is calculated based on cell operating temperature (T_{cell}) in °C using Eq. (19).

$$\eta_{GaAs} = 0.308 - 0.0008 * T_{cell} \tag{19}$$

Total electric output of the system (Q_{GaAs}) is calculated based on the amount of radiation incident upon the cells as determined by

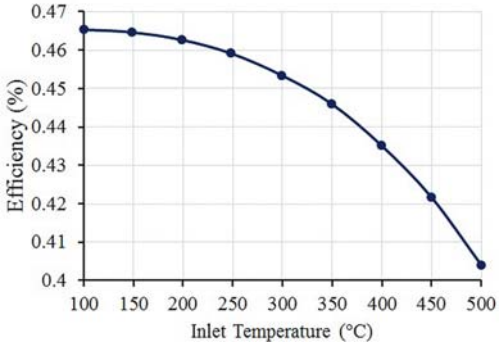

Fig. 13. High temperature thermal efficiency versus inlet temperature.

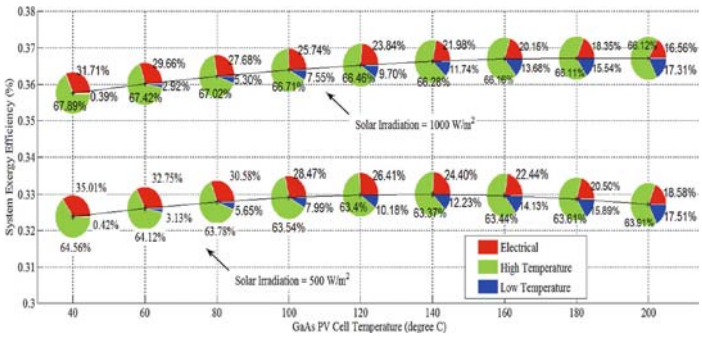

Fig. 14. System exergy efficiency breakdown by components.

Fig. 15. Hybrid PV/T prototype during testing.

the optical model using Eq. (20).

$$Q_{GaAs} = \eta_{GaAs} * G_{cell\_inc} \tag{20}$$

Thermal gain by the low temperature stream ($Q_{low\ temperature\ stream}$) is calculated with the assumption that all light absorbed by the GaAs cells that is not converted to electricity is captured as heat. Bulk radiative losses (Q_{bulk_loss}) from the low temperature thermal stream (minichannels, GaAs cells, and all piping) are included in this model and the output is calculated according to Eq. (21).

$$Q_{low\ temperature\ stream} = \dot{G}_{cell\_abs} - \dot{Q}_{GaAs} - \dot{Q}_{bulk\_loss} \tag{21}$$

Heat loss from the receiver end cap was calculated in SolidWorks [35] and incorporated into our model (see Fig. 10). All losses were taken from the high temperature stream. For a high temperature inlet of 500 °C and low temperature inlet of 200 °C, radiative loss from the inside of the receiver end cap was 42 Watts, and conductive/convective heat loss through two inches of fiberglass insulation on the exterior of the cap was 51 Watts.

Energy efficiency from the high and low temperature streams (η_{energy}) is calculated as per Eq. (22).

$$\eta_{energy} = \frac{\dot{m} c_p (T_{out} - T_{in})}{G} \tag{22}$$

To consider the value of heat produced at different temperatures and the electricity produced by the cells, we evaluate the exergy efficiency ($\eta_{exergy,\ system}$) of the system. Exergy is the maximum usable work that can be extracted from a system at elevated temperature as it comes to equilibrium with a colder heat reservoir. We accomplish this by determining the maximum theoretical usable work that can be extracted from each production stream [Carnot efficiency]. By combining the high ($\eta_{energy,\ high\ temp}$) and low ($\eta_{energy,\ low\ temp}$) temperature stream exergy efficiencies (energy efficiency multiplied by Carnot efficiency) and adding the electrical efficiency, we can determine the total system exergy efficiency as seen in Eqs. (23) and (24).

$$\eta_{exergy\ system} = \eta_{\text{energy, hight emp}} \cdot \eta_{Carnot} + \eta_{\text{energy, low temp}} \eta_{Carnot} + \eta_{GaAs} \tag{23}$$

$$\eta_{Carnot} = 1 - \frac{T_{cold}}{T_{hot}} \tag{24}$$

Essentially, this is the gross system efficiency if we send both thermal streams through an ideal heat engine and add the pure electrical work produced by the solar cells.

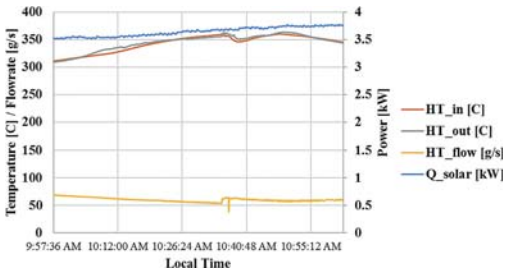

Fig. 16. Temperature and flowrate of March 27 test.

4. System performance testing

The experiment was performed at University of California Merced's Castle Research Center. The latitude and longitude for the location are 37.3°N, and 120.6°W, respectively. Different state variables are measured for the purpose of system performance evaluation and safe operation including solar irradiance, ambient temperature, flow rate, pressure, and fluid temperature. The data is collected at 5 s intervals. Table 4 lists the type and specification of sensors used in the solar and environmental testing rig for each measurement of interest. Direct normal irradiance (DNI) was measured using a mounted normal incidence pyrheliometer. The ambient temperature was measured using a K-type thermocouple inside a radiation shield. The fluid temperature was measured by heavy duty K-type thermocouple sensors where a clusters of three sensors used at inlet and outlet of receiver. The mass flow rate was measured by Coriolis mass flow meter.

The pressure required to keep Therminol VP-1in a liquid state at 400 °C is approximately 1.17 MPa (170 psi). Pressure was applied by nitrogen from a nitrogen tank via the expansion tank which also blanketed the system to prevent oxidation of the oil at elevated temperatures. The system was designed for a flow rate of 50 g/s, or about 1 gallon per minute. At this flow rate, the oil was expected to rise by 10 °C through the solar collector (at 400 °C and 800 W/m^2 DNI).

At the inlet and outlet of the receiver a cluster of three thermocouples was installed in the flow path to accurately measure the temperature rise of the heat transfer fluid across the receiver. The hybrid PV/T system and high temperature loop are shown in Figs. 11 and 12, respectively. The fluid used in the low temperature loop to cool the cells was Duratherm 600. It was circulated and regulated by a Chromalox micro-Therm temperature control system. Flowrate was measured by a Coriolis mass flow meter and temperature was measured via thermocouple clusters positioned as close as possible to the inlet and outlet connections at the receiver.

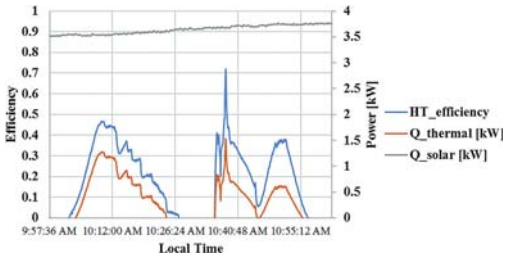

Fig. 17. Generated thermal power and efficiency of March 27 test.

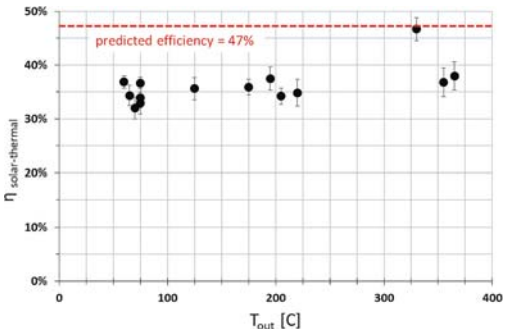

Fig. 18. Solar thermal efficiency results, where black dot is experimental results, dashed line is model results.

5. Results and discussions

5.1. Modelling results

Fig. 13 shows the modelled energy efficiency of the high temperature stream.

In Fig. 14, the different components of the total system exergy efficiency are presented for varying GaAs solar cell temperature for two scenarios of 1000 w/m^2 and 500 w/m^2 DNI. The high temperature stream is assumed to be at 500 °C. The center point of each pie in the plot is the total system exergy (summation of electrical, low temperature, and high temperature exergy components) for varying solar cell temperatures. The black line connects the centers of the related pies and shows the trend of total system exergy with cell temperature. In general, higher solar irradiation results in higher exergy efficiency, with a maximum system exergy efficiency of 0.37 at 200 °C cell temperatures and 1000 W/m^2 DNI.

The percentage values shown in Fig. 14 represents how much each component (i.e., high temperature) contributes to the total system exergy. The high temperature stream contributes most to the total exergy (67% at high solar irradiation), while the low temperatures stream contributes the least (between less than 0.4%–17.3% at high solar irradiation). For example, if the solar cell temperature is maintained at 100 °C in the 500 W/m^2 DNI scenario, the total system exergy is 33%. The solar cells contribute 28.47% to the total system exergy and therefore the direct solar to electric efficiency is 9.4% (multiplication of 28.47% by 33%).

5.2. Experimental results

Tests were conducted under a variety of solar and environmental conditions ranging from low to high DNI and at outlet

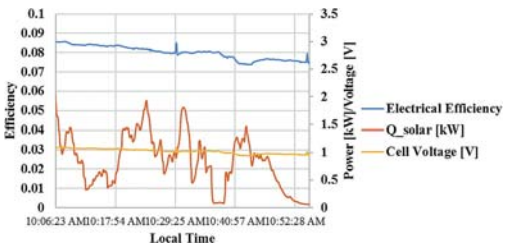

Fig. 19. Direct solar to electric efficiency of GaAs cells (March 20, 2015).

Table 4
Measurements, type and specification of sensors.

Measurements	Quantity	Sensor	Calibration range	Instrument uncertainty	Manufacturer
Ambient temperature	1	Thermocouple, Type k	Up to 1335 °C	greater of 2.2 °C or 0.75%	Omega[a]
System Pressure	2	Pressure Gauge	103 MPa	±1% full scale	Ashcroft[b]
Fluid temperature	18	Thermocouple, Type k	Up to 1335 °C	greater of 2.2 °C or 0.75%	Omega[a]
Mass flow rate	1	Coriolis mass flow meter	0–83 kg/s	±0.1% of reading	Yokogawa Corporation of America[c]
Direct normal irradiance (DNI)	1	Normal Incidence Pyrheliometer	Field of View 5° and sensitivity approx. 8 mV/Wm^{-2}	less than 1%	The Eppley Laboratory, INC.[d]

[a] http://www.omega.com/pptst/TJ36-ICIN.html.
[b] http://www.ashcroft.com/.
[c] http://www.yokogawa.com/us/products/field-instruments/flow-meters/coriolis-flow-meter.htm#details:features.
[d] http://www.eppleylab.com/instrumentation/normal_incidence_pyrheliometer.htm.

temperatures of the high temperature stream between 60 °C and 365 °C. The data analyzed in this article was collected from March 9, 2015 to March 27, 2015 and the combined results of all tests are presented later.

5.2.1. High temperature thermal efficiency

As an example we present the test conducted on March 27 below in Figs. 15–17. This was the highest temperature test and was performed under clear sunny conditions (see Fig. 15). Fig. 16 shows the high temperature inlet and outlet [HT_in, HT_out] profiles and flow rate [HT_flow] at the absorber for the 365 °C test, under a maximum total solar input to the system [Q_solar] of about 4 kW. In Fig. 17, the incoming solar power [Q_solar] as well as the calculated thermal power output [Q_thermal] and efficiency [HT_Efficiency] of the high temperature stream are shown. The maximum thermal energy generated was about 1.25 kWth and the peak efficiency was around 47%. At about 10:36 a.m., we added pressure to the system which caused a temporary drop in flow rate as shown in Fig. 16 and a corresponding spike in efficiency as seen in Fig. 17. We do not consider the data locally around this spike as valid test data. The errors present in the measurements are listed in Table 4. The uncertainty introduced into the calculations of Q_thermal [kW] is approximately ±0.2% and the uncertainty of efficiency calculations is ±2%.

The results of all high temperature thermal tests are plotted with respect to the outlet temperature in Fig. 18. On average the thermal efficiency of the experiment was around 37%, which is lower than the 47% efficiency predicted by the model (see Fig. 13). We discuss causes for the lower than expected efficiency in Section 5.2.3. The 47% efficiency at 330 °C is sort of an anomaly. We have looked at the data for that test and there is no clear reason (solar and flow rate were very stable) for the increased efficiency. The data is included for completeness. The maximum uncertainty as shown in the error bars in Fig. 18 is 2.7%.

5.2.2. PV electrical efficiency

The best direct electrical efficiency data obtained was on March 20th under highly cloudy conditions. The output voltage of the PV cell [Cell Voltage] was measured and electrical efficiency calculated and the results are shown in Fig. 19. The maximum electrical efficiency was around 8%, the short circuit current (I_{sc}) was 230 mA and the fill factor (FF) was determined to be 84.3%.

5.2.3. Experimental limitations and issues

The main challenges we faced during this experiment were failure of the elevation actuator on the tracker, less than ideal mechanism for attaching the solar cells to the cooling channels, and the inability to pull a strong vacuum in the receiver.

Without a working elevation actuator, we could only get full illumination of the receiver tube at a specific time in the morning each day. Subsequent tests only saw partial illumination due to increased sun angle. To account for this, all thermal power and efficiency calculations are elevation corrected to normalize to full illumination of the receiver tube (measured thermal output is divided by measured percentage of tube length that is illuminated).

Our methods for attaching the solar cells to the cooling channel using Omega Therm was not as robust as desired. The adhesive properties of the paste were lost after extended evacuation and heating. Another major problem we had was the inability to pull a strong vacuum (E^{-5} mbar) due to leaks in the vacuum connections, leaks in internal tube assembly, and outgassing.

To account for heat loss caused by an inadequate vacuum we corrected all the high temperature thermal efficiencies. Heat loss measured from the absorber at temperature prior to the test is added to the thermal gain during test to adjust to zero net heat loss. As a result of these corrections, the efficiency versus temperature graph in Fig. 18 is flat and does not decrease with temperature as one would expect in a perfect evacuated system due to radiative loss.

6. Conclusion

A novel double-stage hybrid concentrated PV/T solar system to simultaneously generate electricity and high temperature dispatchable heat has been designed, simulated, fabricated, and tested. Using nonimaging optics, a 5 m wide parabolic trough collector is transformed into an integrated spectrum-splitting device by placing spectrum-sensitive GaAs solar cells on a secondary reflector. The GaAs cells are part of a wide angle secondary concentrator and generate electricity directly while also providing additional concentration towards the high temperature absorber by reflecting sub-bandgap photons. The cells are actively cooled to provide low grade heat. The spectrally selective properties of GaAs cells are used to maximize the exergy output of the system, resulting in a system exergy efficiency of 37%.

One key aspect of the design is that it provides enough geometric concentration on the receiver to maintain high efficiency at operating temperature. This unique design achieves ~60× concentration ratio from parabolic aperture to high temperature absorber, which is significantly higher than conventional parabolic trough concentration ratio and helps the thermal absorber to achieve up to 500 °C even under partial utilization of the solar spectrum. While initially we designed for a 200 °C operating temperature of the cells, modelling indicates that this adds little to the total system exergy while increasing system complexity. Based on these results we conducted the experiment at low solar cell operating temperatures for cooling purpose only. In this design the GaAs cells occupy 2.4% of primary concentrator aperture area and

still receive 41.6% of the incoming direct beam irradiance incident on the trough, making the system cost more affordable. By collecting as much solar energy as we can, this design has the potential to significantly improve the exergy output of future parabolic trough plants.

The experiment was conducted under a variety of solar and environmental conditions and we simultaneously generating electricity from the PV cells and dispatchable high temperature thermal energy from the remaining solar energy [36]. Due to the properties of Therminol VP-1, we were only able to reach a maximum outlet temperature of 365 °C, which is lower than our proposed and modelled target but very close to the outlet temperature of typical parabolic trough CSP plants. On average, the thermal efficiency of the experiment was around 37% which is lower than the 47% efficiency predicted by the model. The maximum electrical efficiency was found to be around 8%, which has room for improvement in future work. The main reasons for the differences between the experimental results and the model output are imperfections of the prototype receiver tube (i.e., cell attachment mechanism, leaks in the vacuum connections, leaks in internal tube assembly, outgassing, formation of condensation), problems with the dual axis tracker, and imperfections in the primary mirror. Future work [37,38] includes replacing the heat transfer fluid with a novel material that will allow us to reach higher temperatures, as well as developing better methods for manufacturing and assembling the receiver (e.g., cell attachment mechanism, better vacuum quality). All of these improvements are currently being implemented in our new project funded by the U.S Department of Energy.

Acknowledgements

The authors are grateful for guidance and financial support from the Advanced Research Projects Agency - Energy (ARPA-E) under grant ARPA-E DE-AR0000464 awarded by the US Department of Energy (DOE) and Southern California Gas Company to develop this system.

References

[1] S. Report, I. Panel, C. Change, Renewable Energy Sources and Climate Change Mitigation: Special Report of the Intergovernmental Panel on Climate Change, vol. 49, 2012, http://dx.doi.org/10.5860/CHOICE.49-6309.
[2] E.C. Kern Jr., & Russell MC. Combined photovoltaic and thermal hybrid collector systems. 13th IEEE Photovolt. Spec., Washington, DC, USA: Massachusetts Inst. of Tech., Lexington (USA). Lincoln Lab.; 1978, p. COO – 4577–3; CONF – 780619–24.
[3] N. Aste, G. Chiesa, F. Verri, Design, development and performance monitoring of a photovoltaic-thermal (PVT) air collector, Renew. Energy 33 (2008) 914–927, http://dx.doi.org/10.1016/j.renene.2007.06.022.
[4] P.G. Charalambous, G.G. Maidment, S.A. Kalogirou, K. Yiakoumetti, Photovoltaic thermal (PV/T) collectors: a review, Appl. Therm. Eng. 27 (2007) 275–286, http://dx.doi.org/10.1016/j.applthermaleng.2006.06.007.
[5] T.T. Chow, A review on photovoltaic/thermal hybrid solar technology, Appl. Energy 87 (2010) 365–379, http://dx.doi.org/10.1016/j.apenergy.2009.06.037.
[6] T.T. Chow, G.N. Tiwari, C. Menezo, Hybrid solar: a review on photovoltaic and thermal power integration, Int. J. Photoenergy (2012) 2012, http://dx.doi.org/10.1155/2012/307287.
[7] A. Ibrahim, M.Y. Othman, M.H. Ruslan, S. Mat, K. Sopian, Recent advances in flat plate photovoltaic/thermal (PV/T) solar collectors, Renew. Sustain Energy Rev. 15 (2011) 352–365, http://dx.doi.org/10.1016/j.rser.2010.09.024.
[8] J. Joe, S. Iniyan, R. Goic, Flat plate solar photovoltaic – thermal (PV/T) systems: a reference guide, Renew. Sustain Energy Rev. 51 (2015) 62–88, http://dx.doi.org/10.1016/j.rser.2015.06.022.
[9] A. Kumar, P. Baredar, U. Qureshi, Historical and recent development of photovoltaic thermal (PVT) technologies, Renew. Sustain Energy Rev. 42 (2015) 1428–1436, http://dx.doi.org/10.1016/j.rser.2014.11.044.
[10] R. Kumar, M.A. Rosen, A critical review of photovoltaic-thermal solar collectors for air heating, Appl. Energy 88 (2011) 3603–3614, http://dx.doi.org/10.1016/j.apenergy.2011.04.044.
[11] L. Zhang, D. Jing, L. Zhao, J. Wei, L. Guo, Concentrating PV/T hybrid system for simultaneous electricity and usable heat generation: a review, Int. J. Photoenergy (2012) 2012, http://dx.doi.org/10.1155/2012/869753.
[12] N. Aste, C. del Pero, F. Leonforte, Water flat plate PV-thermal collectors: a review, Sol. Energy 102 (2014) 98–115, http://dx.doi.org/10.1016/j.solener.2014.01.025.
[13] Mohd Yusof Othman, et al., Photovoltaic-thermal (PV/T) technology–The future energy technology, Renew. energy 49 (2013) 171–174.
[14] Karima E. Amori, Mustafa Adil Abd-AlRaheem, Field study of various air based photovoltaic/thermal hybrid solar collectors, Renew. Energy 63 (2014) 402–414.
[15] Mohd Yusof Othman, et al., Performance analysis of PV/T Combi with water and air heating system: an experimental study, Renew. Energy 86 (2016) 716–722.
[16] Oussama Rejeb, Houcine Dhaou, Abdelmajid Jemni, A numerical investigation of a photovoltaic thermal (PV/T) collector, Renew. Energy 77 (2015) 43–50.
[17] Joe S. Coventry, Performance of a concentrating photovoltaic/thermal solar collector, Sol. Energy 78 (2005) 211–222.
[18] LESO-PB/EPFL, A.G. Enecolo, A.G. Ernst Schweizer, New Generation of Hybrid Solar PV/T Collectors, Swiss Federal Office of Energy, 2000, pp. 1–55.
[19] E. Skoplaki, J.A. Palyvos, On the temperature dependence of photovoltaic module electrical performance: a review of efficiency/power correlations, Sol. Energy 83 (2009) 614–624, http://dx.doi.org/10.1016/j.solener.2008.10.008.
[20] M. Abdelhamid, R. Singh, A. Qattawi, M. Omar, I. Haque, Evaluation of on-board photovoltaic modules options for electric vehicles, IEEE J. Photovolta. 4 (2014) 1576–1584, http://dx.doi.org/10.1109/JPHOTOV.2014.2347799.
[21] M. Abdelhamid, A. Qattawi, R. Singh, I. Haque, Comparison of an analtical hierarchy process and fuzzy axiomatic design for selecting appropriate photovoltaic modules for onboard vehicle design, Int. J. Mod. Eng. 15 (2014) 23–35.
[22] M. Brogren, P. Nostell, B. Karlsson, Optical efficiency of a PV-thermal hybrid CPC module, in: Eurosun 2000-ISES Europe Solar Conference, 2000. Copenhagen. 625.
[23] Chengdong Kong, Zilin Xu, Qiang Yao, Outdoor performance of a low-concentrated photovoltaic–thermal hybrid system with crystalline silicon solar cells, Appl. Energy 112 (2013) 618–625.
[24] M. Li, X. Ji, G.L. Li, S.X. Wei, Y.F. Li, F. Shi, Performance study of solar cell arrays based on a trough concentrating photovoltaic/thermal system, Appl. Energy 88 (9) (2011) 3218–3227.
[25] D.A. Harper, R.H. Hildebrand, R. Stiening, R. Winston, Heat trap: an optimized far infrared field optics system, Appl. Opt. 15 (1976) 53–60, http://dx.doi.org/10.1364/AO.15.000053.
[26] Reflec Tech I. ReflecTech Mirror Film Technical Data 2012. http://www.reflectechsolar.com/pdfs/TechnicalData(ReflecTech).pdf (Accessed 26 August 2015).
[27] R. Winston, Solar Collectors with Evacuated Receiver and Nonimaging External Reflectors, US20040261788 A1, 2004.
[28] F. Burkholder, C.F. Kutscher, Heat Loss Testing of Schott's 2008 PTR70 Parabolic Trough Receiver, 2009.
[29] Coated Steel Tube, Himin Solar Co. Ltd. n.d. http://www.himinsun.com/6-coated-steel.html (Accessed 26 August 2015).
[30] T.J. Silverman, M.G. Deceglie, B. Marion, S. Cowley, B. Kayes, S. Kurtz, Outdoor performance of a thin-film gallium-arsenide photovoltaic module. Conf Rec IEEE Photovolt Spec Conf 2013: 103–108. http://dx.doi.org/10.1109/PVSC.2013.6744109.
[31] MIRO-SUN® Test Report - alanod-solar.de, 2010, pp. 1–20. http://www.bluetec.eu/sites/default/files/pictures/MIRO_SUN_engl_101112_1.pdf (Accessed 25 August 2015).
[32] LightTools Illumination Design Software, https://optics.synopsys.com/lighttools/(Accessed 25 July 2016).
[33] Randy Gee, Randy Brost, Guangdong Zhu, Gary Jorgensen, An improved method for characterizing reflector specularity for parabolic trough concentrators, in: Proceedings of Solar PACES Conference Perpignan (France), vol. 2124, 2010. http://www.reflectechsolar.com/pdfs/CharacterizingReflectorSpecularityforParabolicTrough(SolarPACES)2010.pdf.
[34] MATLAB, http://www.mathworks.com/products/matlab/?requestedDomain=www.mathworks.com.
[35] SOLIDWORKS, http://www.solidworks.com/.
[36] R. Winston, E. Yablonovitch, L. Jiang, B.K. Widyolar, M. Abdelhamid, G. Cranton, D. Cygan, A. Kozlov, "Hybrid solar collector using nonimaging optics and photovoltaic components", Proc. SPIE 9572, Nonimaging Optics: Efficient Design for Illumination and Solar Concentration XII, 957208 (August 25, 2015), 2015, http://dx.doi.org/10.1117/12.2191943.
[37] D. Cygan,, H. Abbasi, A. Kozlov, J. Pondo, R. Winston, B. Widyolar, L. Jiang, M. Abdelhamid, A.P. Kirk, M. Drees, H. Miyamoto, V.C. Elarde and M.L. Osowski, Full Spectrum Solar System: Hybrid Concentrated Photovoltaic/Concentrated Solar Power (CPV-CSP), A Journal of the Materials Research Society (MRS) Advances, Available on CJO 2016 http://dx.doi.org/10.1557/adv.2016.512.
[38] Roland Winston, Lun Jiang, Mahmoud Abdelhamid, Bennett K. Widyolar, Jonathan Ferry, David Cygan, Hamid Abbasi, Alexandr Kozlov, Alexander Kirk, Victor Elarde, Mark Osowski, Nonimaging optics maximizing exergy for hybrid solar system, Proc. SPIE 9955, in: Nonimaging Optics: Efficient Design for Illumination and Solar Concentration XIII—Commemorating the 50th Anniversary of Nonimaging Optics, 99550N, September 7, 2016, http://dx.doi.org/10.1117/12.2239139.